Electronic supplementary information

Carbon dot-based tandem luminescent solar concentrator

Lukáš Zdražil,[a] Sergii Kalytchuk,[a] Kateřina Holá,[a] Martin Petr,[b] Oldřich Zmeškal,[c] Štěpán Kment,[a] Andrey L. Rogach[ad] and Radek Zbořil[a]*

[a]Regional Centre of Advanced Technologies and Materials, Department of Physical Chemistry, Palacký University Olomouc, Šlechtitelů 27, 783 71 Olomouc, Czech Republic

[b]Regional Centre of Advanced Technologies and Materials, Department of Experimental Physics, Palacký University Olomouc, Šlechtitelů 27, 783 71 Olomouc, Czech Republic

[c]Faculty of Chemistry, Brno University of Technology, Purkyňova 118, 612 00 Brno, Czech Republic

[d]Department of Materials Science and Engineering, and Centre for Functional Photonics (CFP), City University of Hong Kong, 83 Tat Chee Avenue, Kowloon, Hong Kong S.A.R.

*Corresponding author's e-mail: radek.zboril@upol.cz

Table of Contents

Structural characterization of synthesized CDs

The chemical structure of the prepared carbon dots was studied by X-ray photoelectron spectroscopy (XPS), Fourier-transform infrared spectroscopy (FTIR), and Raman spectroscopy. The composition of the prepared samples as well as the survey scans and high-resolution XPS spectra are presented in Fig. S2. The most intense peak in C 1s high-resolution scans for all three samples appears at 284.6 eV and is related to the C-C (sp^2) bonding in b-CDs, g-CDs, and r-CDs. The peak centered at approx. 285.9 eV also occurs in all three samples and corresponds to C-O, C-N bonds, and to C-S bonding state in the case of b-CDs. The typical band for carbonyl groups located around 288.0 eV is also visible in the XPS spectra of the samples. The most significant difference in high resolution C 1s scan of the prepared samples is in the presence of an intense peak at 289.2 eV in r-CDs sample (Fig. S2f). This peak appeared after sodium hydroxide treatment of g-CDs (formation process of r-CDs) and can be assigned to a rise of another electron-rich tautomer form on the surface of the particles according to Yuan et. al.[1] The nitrogen atom in b-CDs is presented mostly in pyrrolic form (400.3 eV) according to the high-resolution N 1s spectra (Fig. S2g), while g-CDs and r-CDs have a mixture of pyrrolic and pyridinic nitrogen in the structure (Fig. S2h–i). It is important to note, that there is no peak above 402.0 eV, which is typical for nitro groups. It suggests that the nitrogenated perylene from the synthesis was fully reacted and is not presented in g-CDs and r-CDs samples (position of the individual peaks as well as their percentage rate is shown in Table S1).

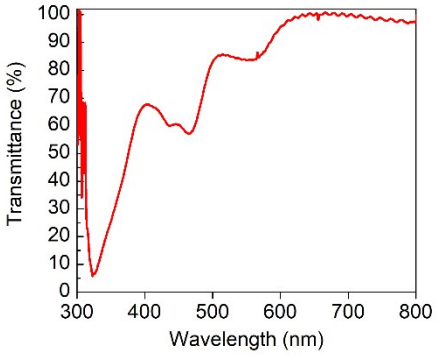

Fig. S1 Transmittance spectrum of carbon dot–based tandem LSC.

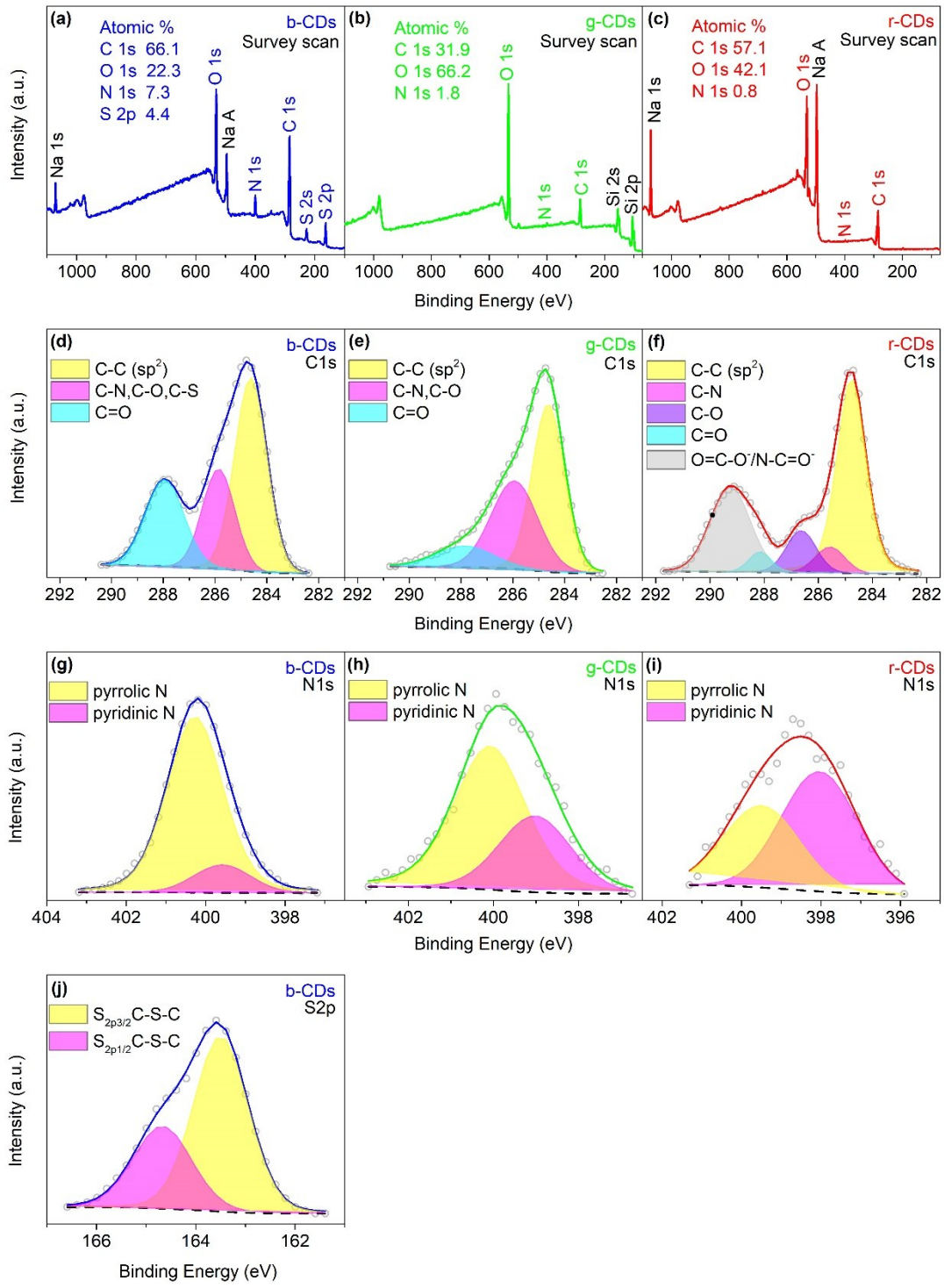

Fig. S2 XPS spectra of prepared carbon dots. (a–c) Survey scan, C 1s (d–f), and N 1s (g–i) high-resolution scans of b-CDs, g-CDs, and r-CDs. (j) S 2p high resolution scan of b-CDs.

Table S1 XPS results.

Chemical state	Sample					
	b-CDs		g-CDs		r-CDs	
	Position (eV)	% rate	Position (eV)	% rate	Position (eV)	% rate
C-C	284.61	49.0	284.63	50.4	284.77	52.4
C-N, C-O, C-S	285.86	25.0	285.94	38.2	285.56, 286.63	16.2
C=O	287.95	26.0	287.85	11.4	288.15	3.7
O=C-O$^-$	-	-	-	-	289.24	27.7
Pyridinic N	399.58	12.5	399.02	32.6	398.03	59.4
Pyrrolic N	400.26	87.5	400.08	67.4	399.50	40.6
C-S-C $S_{2p3/2}$	163.49	66.7	-	-	-	-
C-S-C $S_{2p1/2}$	163.67	33.3	-	-	-	-

FTIR spectra of b-CDs, g-CDs, and r-CDs are presented in Fig. S3a–c. The measurements confirmed presence of oxygen-, nitrogen-, and sulfur-containing functional groups in b-CDs, which is in the good agreement with previously published protocol[2] and XPS measurements. The FTIR spectrum of b-CDs (Fig. S3a) consists of three dominant regions: very broad peaks at 3040 and 3190 cm^{-1} typical for N-H and O-H stretching modes; C=O spectral region typical for carboxylic acid salts at 1630 cm^{-1}, 1515 cm^{-1}, and 1428 cm^{-1}; and broader peak at 1583 cm^{-1} characteristic for aromatic C=C bonding in CDs.[3] The minor bands that occurred in the FTIR spectra at 1210 cm^{-1} and 1075 cm^{-1} are typical for C-N/C-S and C-O stretching modes.[3] Similarly, typical peaks for O-H stretching at 3359 cm^{-1} and for O-H banding mode around 1350 cm^{-1} are presented in Fig. S3b–c. Absorption around 2900 cm^{-1} typical for C-H stretching is also visible in the FTIR scan in g-CDs and r-CDs, respectively. The FTIR spectra of r-CDs exhibited very dramatic decrease in intensity of C-O stretching mode at 1044 cm^{-1} compared to g-CDs. On the other hand, in r-CDs more dominant

peak at region typical for double/aromatic C=C/C=N bonds arises at 1616 cm^{-1} with an intense carbonyl shoulder at 1675 cm^{-1}. This observation confirms the formation of tautomeric form on the surface of the particles, which may cause the red-shift in PL emission after addition of sodium hydroxide (scheme in Fig. 1a).

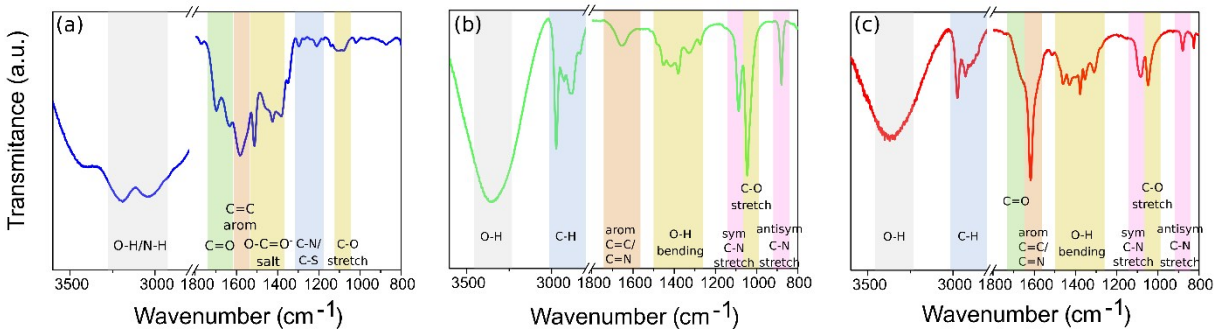

Fig. S3 FTIR spectra of b-CDs, g-CDs, and r-CDs.

Raman spectra of the prepared CDs are presented in Fig. S4. G-band, which is related to the sp^2 bonded carbon in graphite lattice, occurs at 1606 cm^{-1}, 1591 cm^{-1}, and 1586 cm^{-1} for b-CDs, g-CDs, and r-CDs, respectively. Presence of crystal structure defects or surface/edge bonded states was confirmed by presence of the D band at 1308 cm^{-1}, 1308 cm^{-1}, and 1313 cm^{-1} for b-CDs, g-CDs, and r-CDs, respectively.[4]

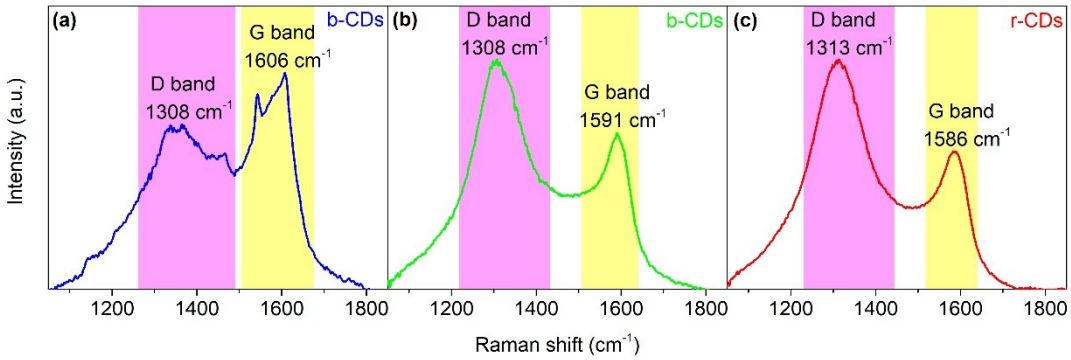

Fig. S4 Raman spectra of b-CDs, g-CDs, and r-CDs.

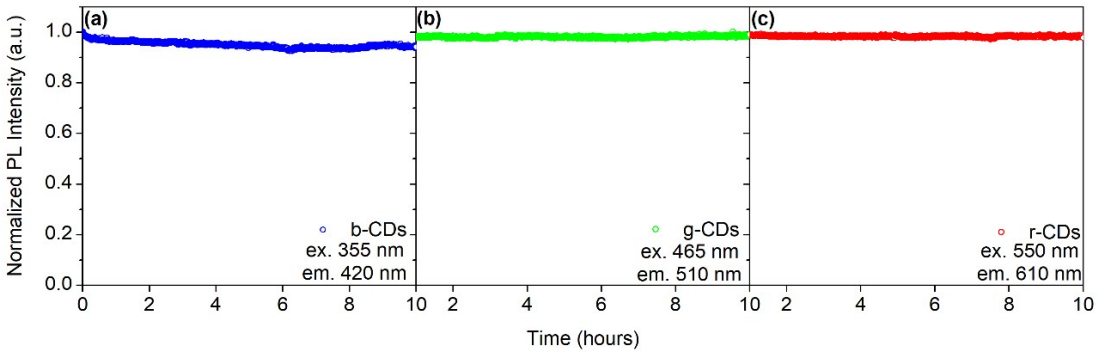

Fig. S5 Photostability of colloidal b-CDs, g-CDs, and r-CDs under 1 mW/cm^2 monochromatic excitation.

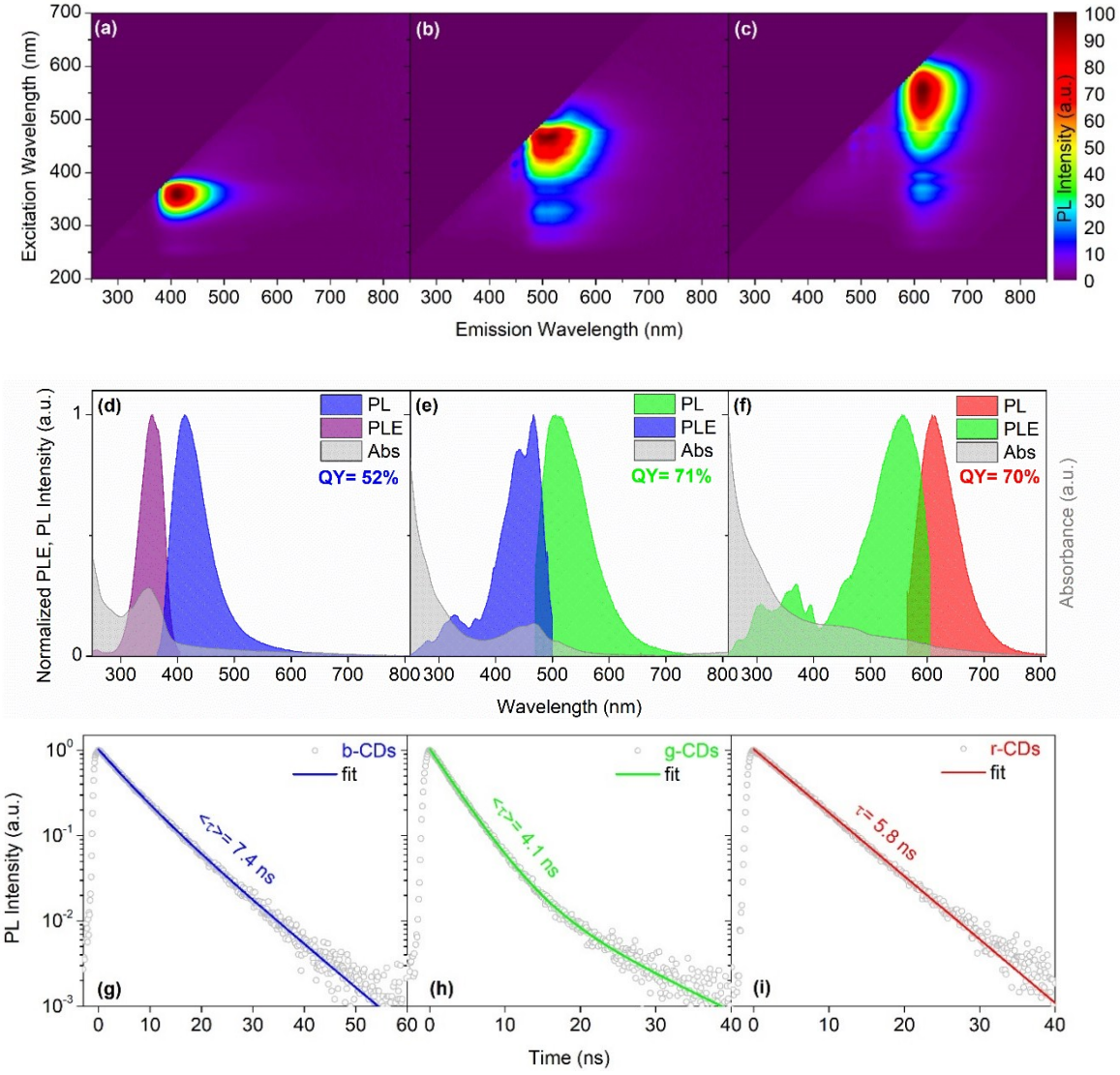

Fig. S6 Optical properties of b-CDs, g-CDs, and r-CDs in polymer matrices. (a–c) Excitation-emission maps. (d–f) Absorption, PL excitation, and PL emission spectra, (g–i) Time-resolved PL decays and the corresponding single and two-exponential fits.

Table S2 The fitting parameters of the corresponding PL decay curves.

Sample	Colloidal Solution	Polymer				
	τ (ns)	B_1 (%)	τ_1 (ns)	B_2 (%)	τ_2 (ns)	<τ> (ns)
b-CDs	9.8	48.2	4.991	51.8	8.630	7.4
g-CDs	3.9	95.8	3.230	4.2	10.166	4.1
r-CDs	5.3	-	-	-	-	5.8

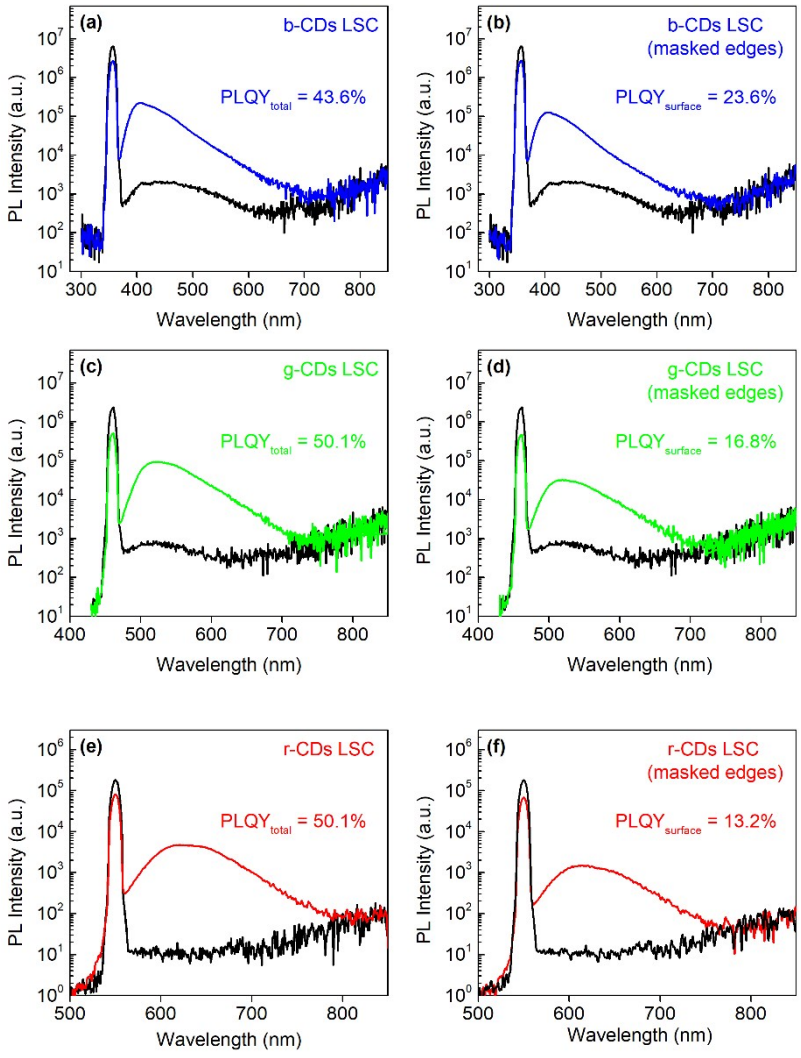

Fig. S7 PL QY measurements of b-LSC (a,b), g-LSC (c,d), and r-LSC (e,f) before and after their edges were masked with a non-transparent black tape.

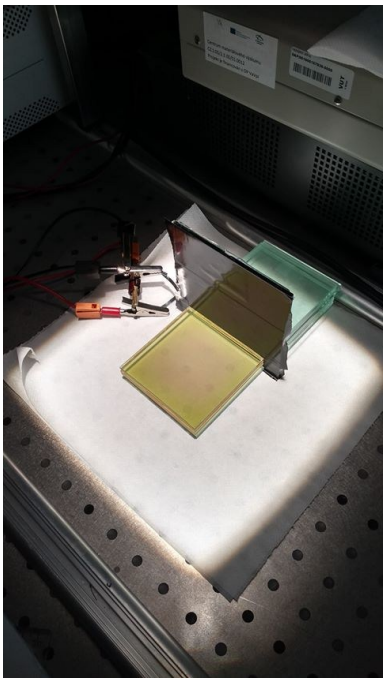

Fig. S8 Experimental setup for electro-optical measurements of tandem LSC coupled to the a-Si solar cell.

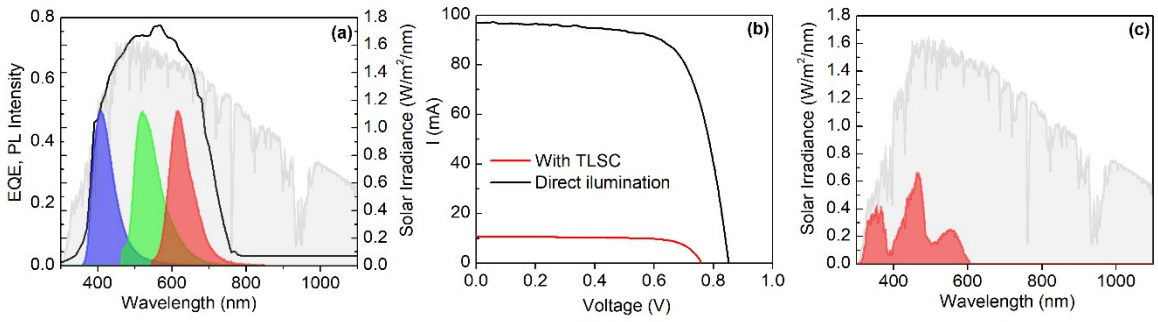

Fig. S9 (a) The EQE spectrum of a-Si solar cell is shown compared with AM 1.5G spectrum. (b) *I-V* measurement of a-Si solar cell and tandem LSC coupled to the same solar cell. (c) Global solar spectrum at air mass 1.5 (highlighted in grey) showing the fraction absorbed by the tandem LSC (highlighted in red).

Table S3 Overview of literature results for LSCs based on semiconductor QDs, perovskite NCs and CDs.

Type of LSC	Type of luminophore	Dimensions (cm)	Light source	η_{int} (%)	η_{ext} (%)	Ref.
single	CdSe/CdS core/shell	2×2×0.2 cm	400 nm	48.0	-	[5]
single	CdSe/CdS core/shell	21.5×1.3×0.5 cm	Solar simulator	10.2	-	[6]
single	$CuInSeS_2In$/ZnS core/shell	12×12×0.3 cm	Solar simulator	16.7	3.27	[7]
single	Silica-coated CdSe/$CdZn_xS_{1-x}$ core/alloyed shell	10×10×0.16 cm	405 nm	24.0	-	[8]
single	Silica-coated CdSe/$CdZn_xS_{1-x}$ core/alloyed shell	10×10×0.16 cm	sunlight	21.0	1.18	[8]
single	PbS/CdS core/shell	10×1.5×0.2 cm	Solar simulator	4.5	1.1	[9]*
single	CDs/PLMA CDs/PVP	10×10×0.1 cm	Solar simulator	4.0	0.4	[10]*
tandem	CDs/PLMA CDs/PVP	10×10×0.1 cm	Solar simulator	-	1.1	[10]*
single	N-CDs	2.5×1.6×0.1 cm	Solar simulator	-	4.75	[11]*
single	Si QDs	12×12×0.26 cm	473 nm	30	2.85	[12]
single	Mn^{2+}-doped perovskite	20×20×0.5 cm	395 nm	7.5	-	[13]
tandem	Mn^{2+}-doped CdSe CISe/ZnS QDs	10×10×0.16 cm	385 nm sunlight	58.0 and 19.0	6.4	[14]
single	N-CDs	2×2×0.2 cm	Solar simulator	-	12.23	[15]*

Type of LSC	Type of luminophore	Dimensions (cm)	Light source	η_{int} (%)	η_{ext} (%)	Ref.
tandem	CDs $CsPb(I_xBr_{1-x})_3$ $CsPb(Cl_xBr_{1-x})_3$	10×10×0.2 cm	Solar simulator	-	3.05	[16]*
single	CNDs	3×3×0.3 cm	354 nm	22.0	12.0	[17]
single	CDs	1.8×1.8×0.11 cm	Solar simulator	-	5.02	[18]*
single	N-CDs	5.0×2.5×0.42 cm	Solar simulator	-	4.52	[19]*
single	PNPLs	10×10×0.2 cm	sunlight	26.0	0.87	[20]
single	CDs	10×10×1 cm	Solar simulator	-	0.92	[21]*
single	CdSe/CdS QDs	10×10×0.4 cm	Solar simulator	-	2.95	[22]*
tandem	CDs + AIE molecules	6.5×2.0×0.2 cm	Solar simulator	-	1.73 and 2.31	[23]*
tandem	CDs + organic dyes	5×5×0.3 cm	Solar simulator	-	4.35 and 11.97	[24]*
tandem	CDs	8×8×0.8 cm	Solar simulator	23.6	2.27	This work

Publications marked with and asterisk (*) do not include Q_{total}, Q_{PL} parameters of used PV cell in formula for optical efficiencies, which may significantly affect the results (In our case, missing Q_{total}/Q_{PL} would increase external quantum efficiency from 2.27% to 4.37%

REFERENCES

1 B. Yuan, S. Guan, X. Sun, X. Li, H. Zeng, Z. Xie, P. Chen and S. Zhou, *ACS Appl. Mater. Interfaces*, 2018, **10**, 16005–16014.

2 Y. Dong, H. Pang, H. B. Yang, C. Guo, J. Shao, Y. Chi, C. M. Li and T. Yu, *Angew. Chem. Int. Ed.*, 2013, **52**, 7800–7804.

3 N. C. Daimay Lin-Vien William Fateley, Jeanette Grasselli, *The Handbook of Infrared and Raman Characteristic Frequencies of Organic Molecules*, Academic Press, 1991.

4 C. J. Reckmeier, J. Schneider, A. S. Susha and A. L. Rogach, *Opt. Express*, 2016, **24**, A312–340.

5 I. Coropceanu and M. G. Bawendi, *Nano Lett.*, 2014, **14**, 4097–4101.

6 F. Meinardi, A. Colombo, K. A. Velizhanin, R. Simonutti, M. Lorenzon, L. Beverina, R. Viswanatha, V. I. Klimov and S. Brovelli, *Nat. Photonics*, 2014, **8**, 392–399.

7 F. Meinardi, H. McDaniel, F. Carulli, A. Colombo, K. A. Velizhanin, N. S. Makarov, R. Simonutti, V. I. Klimov and S. Brovelli, *Nat. Nanotechnol.*, 2015, **10**, 878–885.

8 H. Li, K. Wu, J. Lim, H.-J. Song and V. I. Klimov, *Nat. Energy*, 2016, **1**, 16157.

9 Y. Zhou, D. Benetti, Z. Fan, H. Zhao, D. Ma, A. O. Govorov, A. Vomiero and F. Rosei, *Adv. Energy Mater.*, 2016, **6**, 1501913.

10 Y. Zhou, D. Benetti, X. Tong, L. Jin, Z. M. Wang, D. Ma, H. Zhao and F. Rosei, *Nano Energy*, 2018, **44**, 378–387.

11 Y. Li, P. Miao, W. Zhou, X. Gong and X. Zhao, *J. Mater. Chem. A*, 2017, **5**, 21452–21459.

12 F. Meinardi, S. Ehrenberg, L. Dhamo, F. Carulli, M. Mauri, F. Bruni, R. Simonutti, U. Kortshagen and S. Brovelli, *Nat. Photonics*, 2017, **11**, 177–185.

13 F. Meinardi, Q. A. Akkerman, F. Bruni, S. Park, M. Mauri, Z. Dang, L. Manna and S. Brovelli, *ACS Energy Lett.*, 2017, **2**, 2368–2377.

14 K. Wu, H. Li and V. I. Klimov, *Nat. Photonics*, 2018, **12**, 105–110.

15 X. Gong, W. Ma, Y. Li, L. Zhong, W. Li and X. Zhao, *Org. Electron.*, 2018, **63**, 237–243.

16 H. Zhao, D. Benetti, X. Tong, H. Zhang, Y. Zhou, G. Liu, D. Ma, S. Sun, Z. M. Wang, Y. Wang and F. Rosei, *Nano Energy*, 2018, **50**, 756–765.

17 M. J. Talite, H. Y. Huang, Y. H. Wu, P. G. Sena, K. B. Cai, T. N. Lin, J. L. Shen, W. C. Chou and C. T. Yuan, *ACS Appl. Mater. Interfaces*, 2018, **10**, 34184–34192.

18 Z. Wang, X. Zhao, Z. Guo, P. Miao and X. Gong, *Org. Electron.*, 2018, **62**, 284–289.

19 F. Mateen, M. Ali, H. Oh and S.-K. Hong, *Sol. Energy*, 2019, **178**, 48–55.

20 M. Wei, F. P. G. de Arquer, G. Walters, Z. Yang, L. N. Quan, Y. Kim, R. Sabatini, R. Quintero-Bermudez, L. Gao, J. Z. Fan, F. Fan, A. Gold-Parker, M. F. Toney and E. H. Sargent, *Nat. Energy*, 2019, **4**, 197–205.

21 H. Zhao, *J. Lumin.*, 2019, **211**, 150–156.

22 G. Liu, R. Mazzaro, Y. Wang, H. Zhao and A. Vomiero, *Nano Energy*, 2019, **60**, 119–126.

23 W. Ma, W. Li, R. Liu, M. Cao, X. Zhao and X. Gong, *Chem. Commun.*, 2019, **55**, 7486–7489.

24 F. Mateen, M. Ali, S. Youn, S. Hoon and M. Jae, *Sol. Energy*, 2019, **190**, 488–494.

Author Contributions

L. Z. and K. H. synthesized the samples. L. Z. and K. H. performed material characterization. L. Z. and S. K. conceived and designed the experiments. L. Z. performed optical characterizations. M. P. performed XPS characterization tests. O. Z. performed electro-optical measurements. R. Z. designed and supervised this study. L. Z, S. K., A. R., and R. Z wrote the manuscript. All authors commented on the manuscript.